Macromolecules

Article

pubs.acs.org/Macromolecules

Trans-Rich Structures in Early Stage Crystallization of Polyethylene

Kalman B. Migler,*[,†] Anthony P. Kotula,[†] and Angela R. Hight Walker[‡]

[†]Materials Science & Engineering Division and [‡]Physical Measurements Laboratory, NIST, Gaithersburg, Maryland 20899, United States

ABSTRACT: The kinetic pathway by which molten polymers transform into multi-length-scale, semicrystalline structures upon cooling is critical to their processing, properties, and ultimate performance. However, for the case of polyethylene (PE), critical questions remain concerning early stage kinetics of isothermal crystallization. Here we utilize Raman spectroscopy, in conjunction with turbidity and depolarization measurements, to probe crystallization kinetics in PE because of its unique ability to simultaneously measure intrachain consecutive *trans* conformations (locally straight) and interchain orthorhombic crystallinity. We analyze the spectra within the context of a three-state model to extract the mass fraction of conformations that are locally straight but not part of the orthorhombic crystal, which we term noncrystalline consecutive *trans* (NCCT). We first validate this methodology on the *n*-alkane $C_{21}H_{44}$ where the NCCT mass fraction is expected to be large and then apply it to the early stage crystallization kinetics of PE. We find that the NCCT conformations appear in conjunction with orthorhombic crystallinity, indicating that the growing early stage clusters are rich in NCCT conformations.

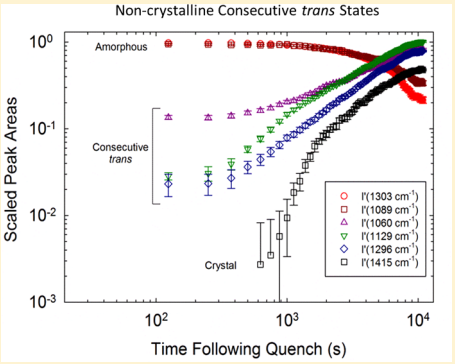

INTRODUCTION

The structure and physical properties of semicrystalline polymers are determined during crystallization, in which the material transforms from an entangled melt into a semicrystalline, multi-length-scale structure.[1] While precise control of crystallization is key to the final properties, it is mainly empirical. Among the broad array of crystallizing polymers, PE holds a special place for economic, scientific, and life-cycle reasons. Despite its maturity, industrial producers continue to develop new strategies to improve properties and processing. Scientifically, PE is important because it is the simplest polymer that forms a crystalline structure, and it serves as a model system for testing our understanding of polymer crystallization in general. A large literature has thus developed for PE devoted to understanding the molten phase, the lamellar semicrystalline state, and the kinetics of the transformation of the former into the latter. Despite much research on PE, there remains vigorous debate on the crystallization pathway. In particular, the events that occur during the early stages of crystallization, known as the precrystalline or induction period, are little understood.

Here we demonstrate that Raman spectroscopy is a powerful tool to probe the kinetics of isothermal crystallization of PE due to its ability to simultaneously measure the evolution of local conformational states and orthorhombic crystallinity. It can be used to measure the mass fraction of conformations that are locally straight but are not part of the orthorhombic crystalline structure, which we call the noncrystalline consecutive *trans* (NCCT) conformation. We are particularly interested in the early time behavior where early stage structures are predicted to be rich in *trans* conformational states that are noncrystalline.

In this work, we first consider the case of an *n*-alkane, $C_{21}H_{44}$, to demonstrate unique ability of Raman spectroscopy to determine the mass fraction of NCCT conformers. By employing an analysis procedure originally developed by Strobl in the CH_2 twist and the CH_2 bend spectral regions,[2] we measure the mass fraction of the NCCT conformers in the crystal, rotator, and melt phases. Having validated the measurement protocol of the NCCT in the well understood *n*-alkane, we use Raman spectroscopy to measure the conformational states during crystallization of PE. We employ simple temperature quenches to transform from the molten phase to a semicrystalline state at undercooling where the kinetics take place over time scales of approximately 1 h and monitor the growth and decay of the Raman bands that are due to amorphous conformations, consecutive *trans* conformations, and orthorhombic crystallinity. We complement these measurements with simultaneous turbidity and depolarized transmitted intensity measurements to gain further insights into the chronology of the crystallization process.

BACKGROUND

A number of models have been proposed to describe the crystallization kinetics of polymers; all invoke the existence of precrystalline structures, either implicitly or explicitly. The most prominent one was developed by Hoffman, Lauritzen, and coworkers at the National Bureau of Standards and pertains to the growth of plate-like crystallites whose surface consists of folded chains.[3,4] This model focuses on the secondary nucleation process, but implicit is the primary nucleation and the formation of embryonic nuclei from which this secondary

Received: December 23, 2014
Revised: June 5, 2015
Published: June 18, 2015

DOI: 10.1021/ma5025895
Macromolecules 2015, 48, 4555−4561

crystallization process occurs. Newer models explicitly invoke structures that are rich in noncrystalline *trans* conformations.[5,6] The spinodal-assisted model by Olmsted and co-workers considers that spatial gradients in the *trans* and *gauche* densities can become amplified, leading to a liquid−liquid phase separated state as a precrystalline structure.[7] Strobl considered the precrystalline structure as a mesomorphic phase that consists of a layer of chain segments that are locally aligned in *trans* conformations but not crystallized.[8−11] Keller and co-workers envisioned a transient phase that is similar to the high-pressure extended-chain phase (mobile hexagonal) phase seen in PE.[12,13] Milner used ideas from polymer brush theory to show that nucleation barriers from melt to rotator phase can be less than that from the melt to crystal.[14] There have also been numerous simulations of PE and alkanes;[15−19] a recent simulation of semidilute PE has indicated that embryonic development begins with the aggregation of noncrystalline, *trans*-rich sequences.[18]

Despite the central role of noncrystalline *trans*-rich conformational states in theoretical constructs of PE crystallization kinetics, few experimental observations have been reported. Sasaki, Tashiro, and co-workers used time-resolved, high-resolution FTIR to monitor conformational changes that occur during early stage crystallization of PE and correlated these measurements with SAXS.[20,21] They deduce that the route to crystallinity proceeds by the random coils transforming into *trans*-rich polymer chains and then into the orthorhombic form. These measurements however did not measure mass fractions and did not differentiate between *trans*-rich structures uniformly distributed in the melt or condensed into a separate state.

Scattering methods that search for precrystalline structures have reported conflicting results. Hsiao et al. found no evidence for large (>10 nm) structures before crystallization,[22] and Li et al., Han, and co-workers found that the SAXS data can be well fit by classical nucleation theory.[23] On the other hand, Akpalu and co-workers showed interesting dependence of undercooling on the evolution of the SAXS, WAXS, and small-angle light scattering signals; of course, the relative sensitivity of these methods must be considered.[24,25] Finally, indirect evidence for *trans*-rich precrystalline precursors in PE come from even-numbered alkanes which do not possess a stable rotator phase but have been shown to pass through a transient rotator phase during quiescent cooling from the melt to the crystal.[26]

Here we exploit the power of Raman spectroscopy to search for noncrystalline *trans*-rich structures in early stage crystallization kinetics in PE. Raman spectroscopy is a widely used technique in the analysis of polymeric materials[2,27−33] and has been applied to online processing of crystallizing fibers[34,35] and film[36,37] but has been little used in isothermal crystallization of polyolefins. Because Raman spectroscopy of PE contains information regarding consecutive *trans* sequences as well as orthorhombic crystallinity, it has great potential to measure the kinetics.

The fundamental Raman band assignments in PE and alkanes have been established in numerous spectral regions;[38−40] here we focus on those in the 1000−1500 cm^{-1} range because of the ability to perform proper normalization of spectra and the ability to derive mass fractions of conformers.[2] The alkanes and PE share numerous bands including those in the C−C stretch (1000−1150 cm^{-1}), the CH_2 twist (1260−1340 cm^{-1}), and the CH_2 bend (1400−1500 cm^{-1}) regions. We first consider the C−C stretch region which contains three intrachain bands: a broad one centered near 1089 cm^{-1} stemming from amorphous conformations and two narrow ones centered near 1060 and 1129 cm^{-1} stemming from the antisymmetric and symmetric consecutive *trans* vibrations. Meier has employed quantum calculations to examine the C−C stretch region for $C_{16}H_{34}$, and the data show that enhancements in the Raman intensity into the two *trans* bands can occur with as few as two consecutive *trans* bonds but that in order to obtain a narrow Raman band, 10 or more consecutive *trans* bonds is required. He qualitatively observed that the Raman intensity with respect to the number of consecutive *trans* bonds in a sequence is nonlinear.[41]

Next, two intrachain peaks can be observed in the CH_2 twist region: a broad one centered near 1304 cm^{-1} which is associated with the amorphous conformational states and a narrow one centered near 1296 cm^{-1} which is associated with consecutive *trans* conformations.[2] Quantum mechanical calculations on *n*-alkanes by Tarazona et al. showed that a conformation consisting of five consecutive *trans* bonds produces the narrow band in the CH_2 twist spectral region whereas various conformations containing two consecutive *trans* bonds produce the broad spectral responses.[42] Summarizing these results, the Raman intensity associated with the consecutive *trans* state begins to appear when there are between three and five consecutive *trans* bonds.

Third, the CH_2 bend mode contains an *inter*chain band near 1415 cm^{-1} that is called the Raman crystallinity band due to a field splitting that occurs when the unit cell is occupied by two structural units.[38−40] This can be used to compute the orthorhombic crystalline mass fraction through normalization.[2] This band is absent in the R_1 rotator phase and triclinic phases of alkanes as well as the mobile hexagonal high-pressure phase of PE.

A useful feature of Raman spectroscopy performed in 180° backscattering mode is that when used with optically transparent substrates, the transmitted light can be utilized for other optical probes, such as measures of optical depolarization, turbidity, or small-angle light scattering, enabling multiprobe experiments. We thus supplement the Raman measurements with simultaneous turbidity and depolarized transmitted intensity, which provides additional information regarding the kinetics.

EXPERIMENTAL SECTION

The optical setup is shown in Figure 1. The Raman measurements are conducted in 180° backscattering mode using a triple grating spectrometer (Horiba T64000) because of the convenience in exploiting the transmitted light for turbidity and depolarization

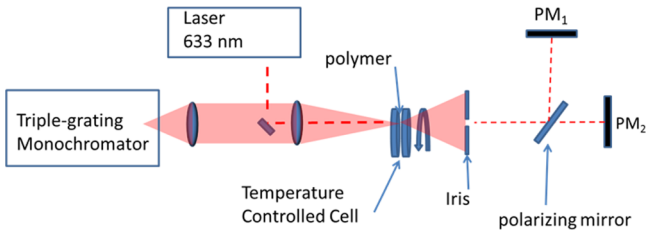

Figure 1. Experimental setup. The Raman scattering is collected in 180° backscattering mode while the turbidity and depolarized transmitted intensity are collected from the transmitted light. Power meters (PM_1 and PM_2) measure the depolarized and polarized transmitted intensity, respectively.

DOI: 10.1021/ma5025895
Macromolecules 2015, 48, 4555−4561

measurements. The spectral resolution is 0.8 cm $^{-1}$. We focus 633 nm vertically polarized light from a HeNe laser onto a spot size roughly 60 μm in diameter at a power level of 15 mW.

The transmitted light is analyzed according to two simple measureands: turbidity and depolarized transmitted intensity ratio. The turbidity is defined through the equation

$$\frac{I_t(t)}{I_0} = e^{-\Lambda(t)z} \quad (1)$$

where Λ is the turbidity (or linear attenuation coefficient), z is the sample thickness, $I_t(t)$ is the intensity of transmitted light, and I_0 is the transmitted intensity at $t = 0$.

Turbidity is caused by nonuniformities in the index of refraction of the material which scatter light away from the incident direction, and in polymer crystallization experiments turbidity is observed at earlier time than signals from conventional techniques.[43,44] In the case of a spherulite growing from the melt with constant radial velocity and no evolution of internal spherulite structure, it was shown that $\Lambda \sim t^4$ though the experimental reality was generally more complex. In a crystallization experiment, one typically assumes that turbidity indicates crystallinity, but if there is a precrystalline structure that causes an index of refraction mismatch with the bulk, then it can also scatter light and cause turbidity. The depolarized transmitted intensity ratio $I_d(t)$ is experimentally defined as

$$I_d(t) = I_\perp(t)/I_t(t) \quad (2)$$

where $I_\perp(t)$ is the intensity of transmitted light with perpendicular polarization to the incident. In the case of early stage crystallization (or precrystallization) containing a random orientation of birefringent domains, the light loses its initial polarization state due to interactions with birefringent domains. In block copolymers, the state of polarization has been modeled as a random walk as the light interacts with successive grains.[45] Depolarization of light, for example as seen by optical microscopy with crossed polarizers, is also frequently used as an indicator of crystallinity, but in principle, birefringent precrystalline structures can also cause depolarized transmitted intensity.

For the sample we utilize NIST SRM 1475, a linear PE with relative molecular mass M_w = 53K and number-average relative molecular mass M_n = 18.3K.[46] Pellets are first melt pressed at 155 °C into disks of thickness 1.0 mm, and the sample is cooled and placed between the quartz disks of a Linkam shear cell, heated to 155 °C, and compressed to the final thickness of 700 μm. Differential scanning calorimetry (DSC) curves at (10 °C/min) show an endothermic peak upon heating at 136 °C and an exothermic crystallization peak at 115.5 °C. The sample thickness is amenable to both the Raman measurements and the early time turbidity and depolarized transmitted intensity measurements. Typical of industrial grade PE, it contains a large number of heterogeneities ($\geq 10^6$ mm^{-3}), and when visualizing crystallization between crossed polarizers in an optical microscope, one tends to observe a "grainy fog" as opposed to distinct spherulitic or axialitic structures, though some surface nucleated spherulites can be observed.[4] Though the present studies are conducted under quiescent (nonflow) conditions, the shear cell provides a future capability for using Raman to study polymers under flow.[47,48]

In 1979, Strobl and Hagedorn introduced a Raman spectroscopy based method, described below, to measure the mass fraction of conformers that are in the NCCT state. They applied this method to PE in its semicrystalline state in order to measure the mass fraction of the *intermediate phase*, i.e., thin spatial regions located between crystalline and amorphous layers of the lamellar structure, where the conformers are neither fully crystalline nor fully amorphous. Strobl and Hagedorn equate the mass fraction of NCCT conformers, obtained spectroscopically, with the mass fraction of the intermediate phase.

Before using the Raman methodology to measure NCCT conformations during isothermal crystallization of PE, we first validate the methodology by examining a simpler system where we expect the mass fraction of NCCT conformations to be large. We find this step to be necessary because Strobl and Hagedorn's work has been questioned on the basis of whether the reported magnitude of the mass fraction of conformers in the NCCT conformation exceeds their measurement uncertainty.[49,50] As a simpler system, we examine the rotator phase of the *n*-alkane $C_{21}H_{44}$ (heneicosane). This alkane exhibits a single rotator phase (R_1) that occurs in a temperature region between the orthorhombic and melt phases, characterized by a lamellar structure in which the chains are straightened by consecutive *trans* conformations, can rotate about their long axis, and are packed in a weakly orthorhombic structure.[51,52] We thus expect this rotator phase to exhibit a large percentage of conformers in the NCCT state.

The methodology to determine the mass fraction of the NCCT conformers starts with the observation that the integrated Raman cross section in the CH_2 twist spectral region (~1300 cm^{-1}) is invariant with respect to temperature.[2] This allows one to reference all integrated band areas to the integrated twist value, even though the optical properties may change, for example as a result of scattering. We express this relationship as

$$I_{tw} = I(1296\ \text{cm}^{-1}) + I(1304\ \text{cm}^{-1}) \quad (3)$$

where I refers to the integrated area under the curve due to each band. We use I' to indicate that a given spectra has been scaled by I_{tw}.

The conversion from integrated band intensity to mass fraction of conformers is straightforward. First, the mass fraction of the conformers in an amorphous state is simply given by $\alpha_a = I'(1304\ \text{cm}^{-1})$, and the mass fraction of conformers in a consecutive *trans* state α_{ct} is given by $\alpha_{ct} = I'(1296\ \text{cm}^{-1})$. Because of the scaling relation of eq 3 we have that $\alpha_a + \alpha_{ct} = 1$. The Raman intensity from this twist band is from the single chain scattering, regardless of whether that chain sits in a locally orthorhombic crystal structure or not. The mass fraction in the orthorhombic crystal state is given by $\alpha_c = I'(1415\ \text{cm}^{-1})/N_c$, where N_c is an experimentally determined. In the three-state model we make the simple assumption that chain segments exist in one of three states: in the amorphous state, in the orthorhombic crystal state or in the NCCT state.

$$1 = \alpha_c + \alpha_a + \alpha_{ncct} \quad (4)$$

This can be re-expressed as $\alpha_{ncct} = \alpha_{ct} - \alpha_c$, which is a useful expression because it anticipates that the measurement of α_{ncct} is feasible when α_{ct} is sufficiently greater than α_c but becomes difficult when $\alpha_{ct} \approx \alpha_c$ due to experimental uncertainties.

The Raman spectra of $C_{21}H_{44}$ are shown in its three principal phases in Figure 2; they are similar to that previously reported $C_{19}H_{40}$.[53] The melt phase is characterized by a broad band in the C−C stretch (≈1089 cm^{-1}) indicative of the amorphous phase along with two small side bands from the *trans* conformational states that exist in small quantity in the melt. Broad bands are also present in the CH_2

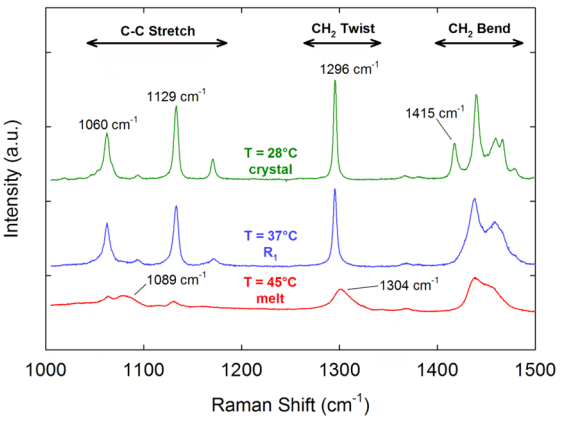

Figure 2. Raman spectra of the alkane $C_{21}H_{44}$ in its melt, rotator, and crystalline phases. Note the presence of the 1415 cm^{-1} band in the crystal phase only and the appearance of the 1296 cm^{-1} band in both the crystal and rotator phases. The curves are scaled by the integrated intensity of the CH_2 twist region.

DOI: 10.1021/ma5025895
Macromolecules 2015, 48, 4555−4561

twist (≈1304 cm^{-1}) and the CH_2 bend regions (≈1440 cm^{-1}). Upon decrease of temperature into the rotator phase, the previously small *trans* bands at ≈1060 and 1129 cm^{-1} dominate the C−C stretch region and the band in the CH_2 twist narrows and moves to lower wavenumber (≈1296 cm^{-1}). In the CH_2 bend region, there is no band indicative of orthorhombic crystallinity. Upon further decrease of temperature into the crystal phase, this band emerges.

For the *n*-alkane, we determine $N_c = 0.56 \pm 0.03$ by assuming 100% crystallinity of the methyl groups. For PE we determine $N_c = 0.62 \pm 0.03$ by matching the value of crystallization observed with Raman spectroscopy with that obtained on DSC using a slow cooled sample of the same polymer. This uncertainty is based on repeated measurements. In the case where there is an intermediate phase, we note that DSC has been reported to overestimate the crystallinity, which could translate into our underestimation of N_c by approximately 10%.[54] Our determination of N_c does exceed that from a previous measurement of $N_c = 0.493$.[30] This systematic uncertainty in N_c does not prevent our study of the NCCT in the case of $\alpha_c \ll \alpha_{ct}$ which we shall show occurs in early stage crystallization but it does limit our ability to examine it when α_c becomes comparable in size to α_{ct}.

For the kinetic experiments, the spectra were collected using a 30 s exposure time. Two spectra were then averaged together in each spectral range (roughly 950−1250 and 1250−1550 cm^{-1}) to obtain adequate signal-to-noise ratio and allow removal of background spikes. We fit the Raman spectra to Lorentzian distributions and fit the amplitude, width, and peak positions along with baseline and linear correction using a nonlinear, least-squares algorithm. We conduct separate fits in the stretch, twist, and bend regions. For the starting parameters, we use peak positions and widths that are found from either later stage crystallinity or early stage melt-like behavior, as appropriate for a given band. This is important for the early stage crystallinity where some of the bands are relatively weak. Experimental uncertainties in the fit parameters are obtained from a MATLAB fitting program, and we use standard error propagation methods in our plots of the mass fractions of conformers. We observed that the fitting procedure under predicts the crystallinity when the crystallinity is less than 0.01 but that the fitted crystallinity is within the uncertainty calculated by the fit. Figures shown without error bars indicate statistical uncertainties that are smaller than the symbol size.

While we adapt the mathematics from Strobl and Hagedorn to measure the mass fraction of conformers in the NCCT state, we use the term α_{ncct} rather than their term α_b because we interpret the former without interpreting the structure whereas the latter refers specifically to the intermediate phase of semicrystalline PE. Figure 3 shows selected intensities (scaled by I_{tw}) for the *n*-alkane as a function of temperature. The orthorhombic crystal band is nonzero only in crystal phase, while the amorphous intensity at (1304 cm^{-1}) increases from 0 to 1 from the crystal to melt phase. The application of the analysis of eqs 3 and 4 on the spectra is shown in Figure 4, where we determine the mass fractions of various conformer states, including the

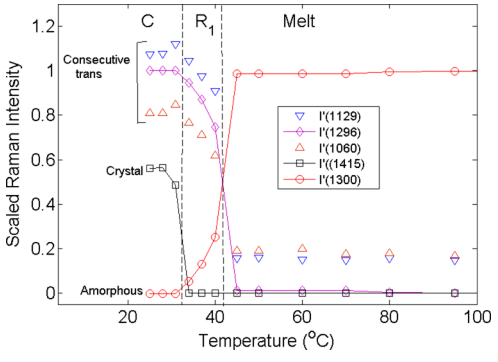

Figure 3. Integrated scaled intensity of selected Raman bands as a function of temperature for $C_{21}H_{44}$ in its crystalline (C), rotator (R_1), and melt (M) phases. Intensity is scaled with respect to the sum of the invariant CH_2 twist vibrational bands at 1296 and 1304 cm^{-1}.

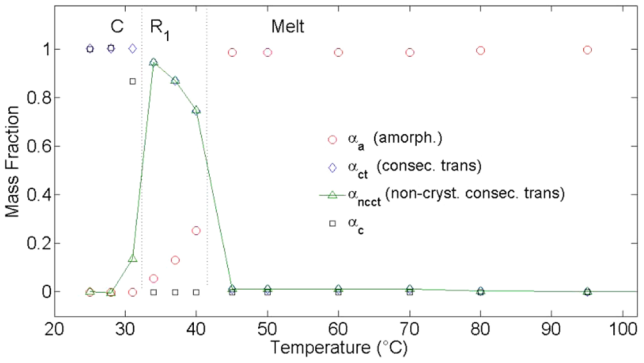

Figure 4. Mass fractions of the various states as a function of temperature for the *n*-alkane $C_{21}H_{44}$. Note that the mass fraction of the NCCT conformers is significantly above zero in the rotator state.

NCCT state. We observe that α_{ncct} is near zero in the crystal phase, jumps to values between 0.96 and 0.75 in the R_1 phase, and then falls to near zero in the melt phase. In the R_1 phase, the relatively large value of α_{ncct} reflects the underlying structure of the rotator phase, discussed previously. The rotator phase also exhibits birefringence and turbidity (not shown). While this analysis on the alkane may be interesting in and of itself, our purpose here is to elucidate how one measures the NCCT mass fraction by providing an example where it is large and then to apply the method to PE crystallization.

Figure 5 shows Raman spectra of PE in the molten phase and semicrystalline state. There are a number of similarities to the spectra

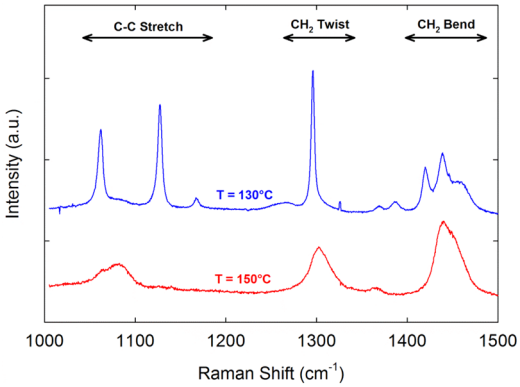

Figure 5. Typical Raman spectra of high-density polyethylene in the semicrystalline state (T = 130 °C) and melt phase (T = 150 °C). The curves are scaled by the integrated intensity of the CH_2 twist region.

of the alkanes (Figure 2), reflecting the similarity in the molecular environment of the CH_2 groups. In the molten phase of PE we again find broad bands in the stretch, twist, and bend regions. In the highly semicrystalline case, we find these same bands at reduced intensity but also observe the bands indicative of continuous *trans* conformations at 1060, 1129, and 1296 cm^{-1} as well as the orthorhombic crystallinity band at 1415 cm^{-1}. The presence of crystalline and amorphous bands in the semicrystalline sample is broadly understood as reflecting the underlying amorphous−crystalline stacking into a lamellar structure. Unlike $C_{21}H_{44}$, there is no stable rotator phase in PE at atmospheric pressure.

Our general experimental protocol is to measure the kinetics of the crystallization through Raman spectroscopy in conjunction with the turbidity and the depolarized transmitted intensity following a temperature quench from above to below the melting point. We hold the temperature at 155 °C for 5 min and then decrease the temperature at a set rate of 20 °C/min to a value of either 130 or 128 °C. There is a narrow range of final temperatures of only a few degrees

DOI: 10.1021/ma5025895
Macromolecules 2015, 48, 4555−4561

for which these experiments, as currently implemented, are feasible. If the final temperature is too high, either crystallization does not occur or the kinetics is too slow over the time scale of several hours. If the final temperature is too low, then either the Raman is temporally not sensitive enough to capture the rapid kinetics or crystallization becomes sizable before the sample in the cell has reached its final temperature. We calibrated the shear cell with temperature melting point standards and found that the temperature within the viewing window of the cell can vary by ≈0.5 °C. Because of the large variation in crystallization kinetics as a function of temperature and molar mass,[55] along with some pellet-to-pellet variations in molar mass and the small temperature gradient in the shear cell, some sample-to-sample variability in the crystallization kinetics was observed. We minimize it by following identical sample preparation protocols.

Figure 6 shows the evolution of the Raman spectrum in the stretch, twist, and bend regions following a crystallization quench from 155 to

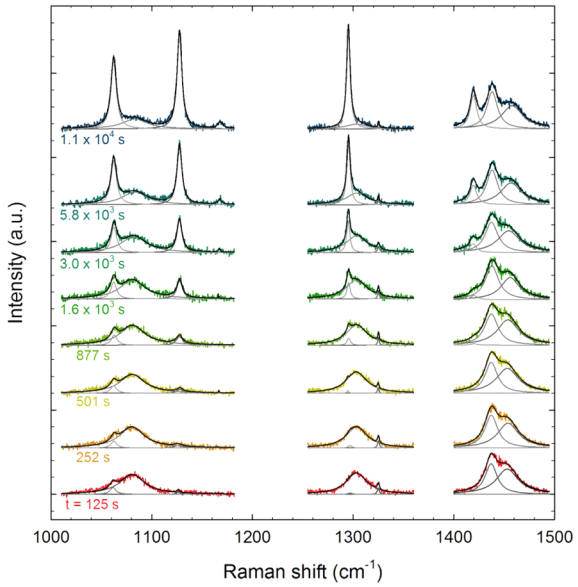

Figure 6. Evolution of Raman spectra of the high density polyethylene following a temperature quench from 155 to 128 °C. Note that the time difference between successive plots increases exponentially. The colored lines indicate the raw data, the overlaying black lines indicate the full curve fits, and the light gray lines indicate the individual Lorentzian fits. The curves are scaled by the integrated intensity of the CH_2 twist region.

128 °C. Note the time between successive plots increases exponentially. The first spectrum at t = 125 s is typical of the melt phase while the last at $t = 1.1 \times 10^4$ s is typical of the semicrystalline state as seen in Figure 5. We observe the growth of bands associated with intrachain consecutive *trans* structures in the C−C stretch (1060 and 1129 cm^{-1}) and CH_2 twist (1296 cm^{-1}) regions along with the reduction of bands associated with the amorphous conformational phases in those same two regions, (1089 and 1304 cm^{-1}). Also, we note the growth of the interchain orthorhombic crystallinity band at 1415 cm^{-1}. In order to examine the relative evolution of the various bands, the fourth and fifth curves at t = 877 and 1.6×10^3 s are useful. At these times, the consecutive *trans* bands at 1060, 1129, and 1293 cm^{-1} are emerging, but there is very little growth in the orthorhombic crystal band at 1415 cm^{-1}.

We next scale these bands by the integrated intensity of the twist region I_{tw}, as was done for the alkane. The results are shown in Figure 7, which is plotted on a double-logarithmic scale. This plot more clearly shows the trends described in the discussion of Figure 6, most notably the increase of intensity of the consecutive *trans* bands prior to the emergence of the orthorhombic crystal band. Also, note the decrease in the two amorphous bands in the bend and twist regions.

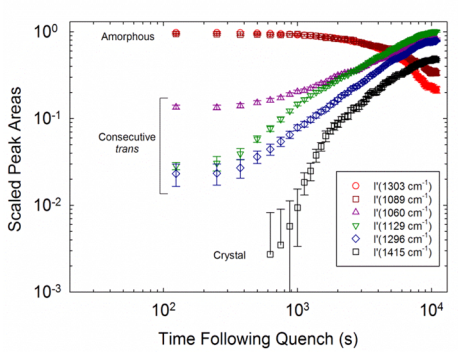

Figure 7. Integrated scaled intensity of selected Raman bands as a function of time following the 155−128 °C temperature quench, extracted from the full data set of Figure 6.

The mass fractions of chain segments in the orthorhombic crystal (α_c), amorphous (α_a), consecutive *trans* (α_{ct}), and the NCCT (α_{ncct}) states as a function of time are reported in Figure 8A. Note in Figure

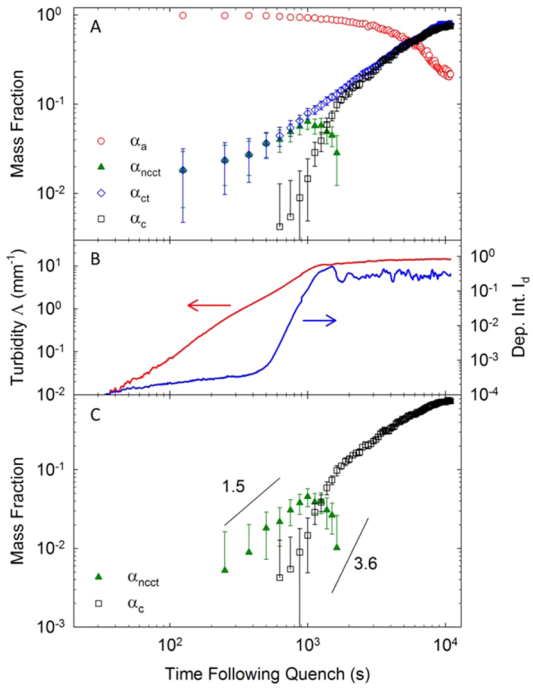

Figure 8. (A) Evolution of the mass fraction of chain segments in the orthorhombic crystalline, the amorphous, and the noncrystalline consecutive *trans* (NCCT) states for HDPE following the 155−128 °C temperature quench, as extracted from data in Figure 7. (B) Turbidity and depolarized transmitted intensity ratio I_d during temperature quench. (C) Data from (A) but with the t = 0 s melt value of α_{ncct} subtracted from $\alpha_{ncct}(t)$.

8A that a small amount of NCCT is present in the melt phase. The orthorhombic crystallinity is first detectable when it reaches a magnitude of $\alpha_c \approx 0.01$, which occurs at $t \approx 1000$ s. The Avrami exponent for the early stage crystallization is $n \approx 3.6 \pm 0.5$, consistent with expectations for this molecular weight range.[55]

The turbidity and depolarized transmitted intensity ratio show earlier time sensitivity to the presence of early crystalline kinetics than the Raman measurements, as shown in Figure 8B. Comparing the growth of the Λ and I_d, we first note that they do not follow the same functional form. We find a power law scaling of $\Lambda \sim t^2$ over a time range from roughly 40 to 1×10^3 s, which ends when crystallinity reaches approximately 6%. In contrast, I_d shows two distinct behaviors

DOI: 10.1021/ma5025895
Macromolecules 2015, 48, 4555−4561

at early times. Over a time range of roughly 40−1000 s, where the NCCT state grows but the crystallinity is not detectable (less than 0.01), I_d increases with time as a power law of roughly $t^{0.4}$. But once the crystallinity starts to become observable, the power law jumps to approximately t^8.

In order to compare the magnitude of α_{ncct} that is due to the growing structures to α_c, we replot the data from Figure 8A but subtract from α_{ncct} the value that is associated with the melt, as shown in Figure 8C. This plot contains the result that at early times when $\alpha_c < 0.05$ the growth of the NCCT conformations coincides with that of the orthorhombic crystallinity and that the value of α_{ncct} exceeds or is comparable to α_c. Thus, the growing early stage clusters are rich in NCCT conformations. The concomitant rise in turbidity indicates that these NCCT conformations are not uniformly distributed in the melt but are contained within the growing clusters. At later times, for $t >$ 1700 s, the uncertainty in the value of α_{ncct} increases as α_c and α_{ct} become comparable in magnitude, as discussed earlier, and we do not report α_{ncct}. The final three data α_{ncct} data points in Figures 8A and 8C do show a downward trend, but due to the increase relative uncertainty in these data points, we do not draw a definitive conclusion regarding this trend.

We have also measured crystallization kinetics for the case of a shallower temperature quench to the final temperature of 130 °C (rather than 128 °C). The results for the mass fractions of the various states and for the optical data are shown in Figure 9. The basic trends

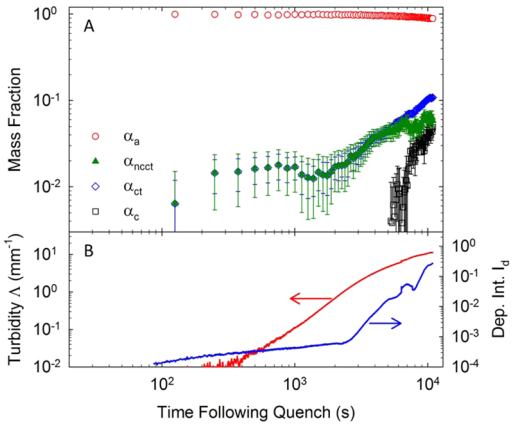

Figure 9. Same as Figure 8 except for the final temperature is 130 °C.

from this data are the same as from the earlier described quench to 128 °C. We still observe during the early stage that the mass fraction of the NCCT exceeds that of the orthorhombic crystal state and that turbidity provides the earliest indication of impending precrystallization and crystallization. The primary difference is that the overall kinetics is much slower, in accord with well-known dependencies of crystallization rate with temperature.[55]

DISCUSSION

These experiments demonstrate the important role of NCCT conformations during early stage heterogeneous crystallization of a linear PE with moderate molar mass distribution. The early stage structure has the following characteristics: it contains consecutive *trans* sequences that are not in an orthorhombic state, as observed by Raman spectroscopy; it grows from the melt in a condensed state, as observed by turbidity; and it consists of chain segments that are locally aligned with each other, as seen by depolarized transmission measurements. We find that in the early stage the mass fraction of NCCT conformers does not exceed 6%. The small value of this quantity may account for the sparse number of reports in the literature on precrystalline conformers in PE. Despite its small magnitude, it may be critical to the kinetic pathway by which PE crystallizes at low undercooling and is important for understanding the thermodynamics of this system.

Our observations of the NCCT conformations along with the observation that it depolarizes and scatters the incident light are consistent with a few structures that have been suggested: a transient rotator phase, a transient hexagonal phase (as seen at high pressure), or a precrystalline embryo that consists of chains locally in both the NCCT and the orthorhombic states.

Other methods, notably WAXS, would be quite useful in ascertaining the structure associated with the NCCT conformations, but this presents experimental challenges for two reasons. First, as discussed above, the mass fraction of the NCCT conformers is small at 6% and, second, for the case of a possible hexagonal phase the position of the 100_h X-ray reflection for PE at melt temperature is expected to differ from that of the 110° by only $2\theta \approx 0.7°$, which might be difficult to resolve in early stage crystallization.[56]

Our results complement and clarify the IR work of Tashiro et al. on isothermal crystallization of PE,[20,21] who monitored a "disordered *trans*" peak and a crystalline peak following a temperature quench. The disordered *trans* was attributed to sequences containing (...$TTG\bar{T}TT$...). Prior to the crystallinity peak, they observed an increase in the disordered *trans* peak, and then once crystallization commences they observe that it decreases. The Raman in contrast is sensitive to the NCCT conformations at early times and allows measurement of mass fractions. Our simultaneous measurements of turbidity and depolarized transmitted intensity then allow us to conclude that the NCCT conformations are nucleated from the melt.

CONCLUSION

The ability of Raman spectroscopy to distinguish consecutive *trans* chain segments that are part of an orthorhombic crystal from those that are not yields important insights into the nature of the polymer crystallization process. We conclude that precrystalline states composed of locally straight, noncrystalline chain segments in conjunction with orthorhombic crystallinity are condensed into a separate state at the earliest stages of crystallization. More work is needed to ascertain which of the proposed crystallization models best matches experimental data. We hope this motivates more work to make explicit predictions regarding the growth of the NCCT conformers during crystallization. On the experimental side, these methods open up further opportunities, for example, to study how the kinetics is influenced by molar mass, its distribution, branching, or flow. Thus, we anticipate that Raman spectroscopy in conjunction with orthogonal techniques will find continued use in unravelling the multi-length and time scale kinetics of polymer crystallization.

AUTHOR INFORMATION

Corresponding Author

*E-mail kalman.migler@nist.gov (K.B.M.).

Notes

The authors declare no competing financial interest.

ACKNOWLEDGMENTS

We acknowledge useful conversations and assistance from Chad Snyder, Amanda McDermott, Jack Douglas, Steven Hudson, Peter Olmsted, Scott Milner, Gert Strobl, and Stephen Cheng. Certain commercial equipment, instruments, or materials are identified in this paper in order to adequately

DOI: 10.1021/ma5025895
Macromolecules 2015, 48, 4555−4561

specify the experimental procedure. Such identification does not imply recommendation or endorsement by the National Institute of Standards and Technology, nor does it imply that the materials or equipment identified are necessarily the best available for the purpose.

REFERENCES

(1) Kimata, S.; Sakurai, T.; Nozue, Y.; Kasahara, T.; Yamaguchi, N.; Karino, T.; Shibayama, M.; Kornfield, J. A. *Science* **2007**, *316* (5827), 1014−1017.
(2) Strobl, G. R.; Hagedorn, W. *J. Polym. Sci., Part B: Polym. Phys.* **1978**, *16* (7), 1181−1193.
(3) Hoffman, J. D.; Lauritzen, J. I. *J. Res. Natl. Bur. Stand. (U. S.)* **1961**, *A 65* (4), 297.
(4) Hoffman, J. D.; Frolen, L. J.; Ross, G. S.; Lauritzen, J. I. *J. Res. Natl. Bur. Stand., Sect. A* **1975**, *79* (6), 671−699.
(5) Cheng, S. Z. D.; Keller, A. *Annu. Rev. Mater. Sci.* **1998**, *28*, 533−562.
(6) Strobl, G. *Prog. Polym. Sci.* **2006**, *31* (4), 398−442.
(7) Olmsted, P. D.; Poon, W. C. K.; McLeish, T. C. B.; Terrill, N. J.; Ryan, A. J. *Phys. Rev. Lett.* **1998**, *81* (2), 373−376.
(8) Strobl, G. *Eur. Phys. J. E* **2000**, *3* (2), 165−183.
(9) Strobl, G. *Eur. Phys. J. E* **2005**, *18* (3), 295−309.
(10) Strobl, G. *Rev. Mod. Phys.* **2009**, *81* (3), 1287−1300.
(11) Sirota, E. B. *Macromolecules* **2007**, *40* (4), 1043−1048.
(12) Keller, A.; Hikosaka, M.; Rastogi, S.; Toda, A.; Barham, P. J.; Goldbeckwood, G. *J. Mater. Sci.* **1994**, *29* (10), 2579−2604.
(13) Rastogi, S.; Hikosaka, M.; Kawabata, H.; Keller, A. *Macromolecules* **1991**, *24* (24), 6384−6391.
(14) Milner, S. T. *Soft Matter* **2011**, *7* (6), 2909−2917.
(15) Sommer, J. U.; Luo, C. F. *J. Polym. Sci., Part B: Polym. Phys.* **2010**, *48* (21), 2222−2232.
(16) Yi, P.; Rutledge, G. C. *J. Chem. Phys.* **2011**, *135* (2), 024903.
(17) Yi, P.; Locker, C. R.; Rutledge, G. C. *Macromolecules* **2013**, *46* (11), 4723−4733.
(18) Lan, Y. K.; Su, A. C. *Polymer* **2014**, *55* (14), 3087−3092.
(19) Stepanow, S. *Phys. Rev. E* **2014**, *90* (3), 032601.
(20) Tashiro, K.; Sasaki, S.; Gose, N.; Kobayashi, M. *Polym. J.* **1998**, *30* (6), 485−491.
(21) Sasaki, S.; Tashiro, K.; Kobayashi, M.; Izumi, Y.; Kobayashi, K. *Polymer* **1999**, *40* (25), 7125−7135.
(22) Wang, Z. G.; Hsiao, B. S.; Sirota, E. B.; Srinivas, S. *Polymer* **2000**, *41* (25), 8825−8832.
(23) Li, J. Y.; Li, W.; Cheng, H.; Zhang, L. N.; Li, Y.; Han, C. C. *Polymer* **2012**, *53* (12), 2315−2319.
(24) Akpalu, Y. A.; Amis, E. J. *J. Chem. Phys.* **2000**, *113* (1), 392−403.
(25) Xiao, Z. C.; Akpalu, Y. A. *Polymer* **2007**, *48* (18), 5388−5397.
(26) Sirota, E. B.; Herhold, A. B. *Science* **1999**, *283* (5401), 529−532.
(27) Maxfield, J.; Stein, R. S.; Chen, M. C. *J. Polym. Sci., Part B: Polym. Phys.* **1978**, *16* (1), 37−48.
(28) Glotin, M.; Mandelkern, L. *Colloid Polym. Sci.* **1982**, *260* (2), 182−192.
(29) Pigeon, M.; Prud'homme, R. E.; Pézolet, M. *Macromolecules* **1991**, *24* (20), 5687−5694.
(30) Mutter, R.; Stille, W.; Strobl, G. *J. Polym. Sci., Part B: Polym. Phys.* **1993**, *31* (1), 99−105.
(31) Naylor, C. C.; Meier, R. J.; Kip, B. J.; Williams, K. P. J.; Mason, S. M.; Conroy, N.; Gerrard, D. L. *Macromolecules* **1995**, *28* (24), 8459−8459.
(32) Lee, Y. J.; Moon, D.; Migler, K. B.; Cicerone, M. T. *Anal. Chem.* **2011**, *83* (7), 2733−2739.
(33) Lee, Y. J.; Snyder, C. R.; Forster, A. M.; Cicerone, M. T.; Wu, W. L. *ACS Macro Lett.* **2012**, *1* (11), 1347−1351.
(34) Paradkar, R. P.; Sakhalkar, S. S.; He, X.; Ellison, M. S. *J. Appl. Polym. Sci.* **2003**, *88* (2), 545−549.
(35) Cakmak, M.; Serhatkulu, F. T.; Graves, M.; Galay, J. *Antec'97 - Plastics Saving Planet Earth* **1997**, *1*−*3*, 1794−1799.
(36) Cherukupalli, S. S.; Ogale, A. A. *Polym. Eng. Sci.* **2004**, *44* (8), 1484−1490.
(37) Gururajan, G.; Ogale, A. A. *J. Raman Spectrosc.* **2009**, *40* (2), 212−217.
(38) Boerio, F. J.; Koenig, J. L. *J. Chem. Phys.* **1970**, *52* (7), 3425.
(39) Gall, M. J.; Willis, H. A.; Hendra, P. J.; Peacock, C. J.; Cudby, M. E. A. *Polymer* **1972**, *13* (3), 104.
(40) Gall, M. J.; Willis, H. A.; Cudby, M. E. A.; Peacock, C. J.; Hendra, P. J. *Spectrochim. Acta, Part A* **1972**, *A 28* (8), 1485.
(41) Meier, R. J. *Polymer* **2002**, *43* (2), 517−522.
(42) Tarazona, A.; Koglin, E.; Coussens, B. B.; Meier, R. J. *Vib. Spectrosc.* **1997**, *14* (2), 159−170.
(43) Heck, B.; Kawai, T.; Strobl, G. *Polymer* **2006**, *47* (15), 5538−5543.
(44) Fritsch, J.; Stille, W.; Strobl, G. *Colloid Polym. Sci.* **2006**, *284* (6), 620−626.
(45) Garetz, B. A.; Newstein, M. C.; Dai, H. J.; Jonnalagadda, S. V.; Balsara, N. P. *Macromolecules* **1993**, *26* (12), 3151−3155.
(46) Hoeve, C. A. J.; Wagner, H. L.; Verdier, P. H. *J. Res. Natl. Bur. Stand., Sect. A* **1972**, *A-76* (2), 137.
(47) Archer, L. A.; Fuller, G. G.; Nunnelley, L. *Polymer* **1992**, *33* (17), 3574−3581.
(48) Chai, C. K.; Dixon, N. M.; Gerrard, D. L.; Reed, W. *Polymer* **1995**, *36* (3), 661−663.
(49) Naylor, C. C.; Meier, R. J.; Kip, B. J.; Williams, K. P. J.; Mason, S. M.; Conroy, N.; Gerrard, D. L. *Macromolecules* **1995**, *28* (8), 2969−2978.
(50) Mandelkern, L.; Alamo, R. G. *Macromolecules* **1995**, *28* (8), 2988−2989.
(51) Sirota, E. B.; King, H. E.; Singer, D. M.; Shao, H. H. *J. Chem. Phys.* **1993**, *98* (7), 5809−5824.
(52) Wentzel, N.; Milner, S. T. *J. Chem. Phys.* **2010**, *132* (4), 044901.
(53) Barnes, J. D.; Fanconi, B. M. *J. Chem. Phys.* **1972**, *56* (10), 5190.
(54) Cheng, J. L.; Fone, M.; Reddy, V. N.; Schwartz, K. B.; Fisher, H. P.; Wunderlich, B. *J. Polym. Sci., Part B: Polym. Phys.* **1994**, *32* (16), 2683−2693.
(55) Ergoz, E.; Fatou, J. G.; Mandelke, L. *Macromolecules* **1972**, *5* (2), 147.
(56) Kolnaar, J. W. H.; Keller, A.; Seifert, S.; Zschunke, C.; Zachmann, H. G. *Polymer* **1995**, *36* (20), 3969−3974.

DOI: 10.1021/ma5025895
Macromolecules 2015, 48, 4555−4561